Imaging of myocardial inflammation with somatostatin receptor based PET/CT — A comparison to cardiac MRI

Constantin Lapa [a,*,1], Theresa Reiter [b,c,1], Xiang Li [a], Rudolf A. Werner [a,c], Samuel Samnick [a], Roland Jahns [b,c,d], Andreas K. Buck [a], Georg Ertl [b,c], Wolfgang R. Bauer [b,c]

[a] Department of Nuclear Medicine, University Hospital Würzburg, Oberdürrbacher Strasse 6, 97080 Würzburg, Germany
[b] Department of Internal Medicine, University Hospital Würzburg, Oberdürrbacher Strasse 6, 97080 Würzburg, Germany
[c] Comprehensive Heart Failure Center, University Würzburg, Straubmühlweg 2a, 97078 Würzburg, Germany
[d] Interdisciplinary Bank of Biomaterials and Data Würzburg, University Hospital Würzburg, Straubmühlweg 2a, Building A8/A9, 97078 Würzburg, Germany

1. Introduction

Macrophages and monocytes play a pivotal role in healing processes of the myocardium [1]. After infarction, they are crucial effectors in orchestration of the balance between inflammation and its resolution [1–5]. Delayed healing has been reported for areas of microvascular obstruction due to impaired macrophage recruitment [1,5]. In myocarditis, the macrophage-triggered immune response is mandatory to fight viral or other agents [6]. Although endomyocardial biopsy remains the gold standard for establishing the diagnosis of myocarditis, its sensitivity is variable and might be as low as 10–35% [7,8].

Magnetic resonance imaging (MRI) is the gold standard in cardiovascular imaging and plays an unequaled role in the non-invasive diagnosis of myocardial inflammation and healing. Contrast-enhanced T1- and T2-weighted sequences allow structural assessment. T2-weighted sequences reveal intra-myocardial edema associated with acute inflammation [9]. The differentiation between acute myocarditis and (sub-)acute infarction is based on distinct features in T2-weighted and contrast-enhanced images. Whereas inflammation can occur throughout the heart and is usually limited to the epi- and myocardium, ischemia also affects the (sub-)endocardium and is confined to the area supplied by the culprit vessel. Microvascular obstruction, an indicator of severe tissue damage, can be detected in re-perfused infarct areas as signal void due to slow contrast penetration secondary to endothelial swelling and embolization by cell debris [10].

Myocardial inflammation can also be visualized effectively using the glucose analog ^{18}F-fluorodeoxyglucose (^{18}F-FDG) in positron emission tomography (PET) as glucose metabolism is activated by enhanced

* Corresponding author.
E-mail address: Lapa_C@ukw.de (C. Lapa).
[1] Both authors contributed equally to the manuscript.

expression of glucose transporters and production of glycolytic enzymes in inflammatory cells [11]. Its use in endocarditis as well as in myocarditis has been reported [12–14]. However, specificity of PET with ^{18}F-FDG is hampered by physiologic ^{18}F-FDG accumulation in healthy myocardium [15]. Activated macrophages have been described to overexpress somatostatin receptor subtypes 1 and 2 (SSTR) on their cell surface during differentiation of monocytes [16,17]. Since these receptors display active binding sites, specific SSTR-targeted radiotracers such as ^{68}Ga-DOTA-TATE or -TOC may be used to directly identify activated macrophages. Recently, inflammation of large arteries has been detected by PET imaging of the somatostatin receptor (SSTR) subtype 2 by demonstrating increased tracer uptake in large vessel artherosclerotic plaques [18,19]. Detection of myocardial inflammatory activity would facilitate making the diagnosis of acute myocarditis in patients in whom conventional imaging is inconclusive and/or endomyocardial biopsies unyielding or not achievable. Furthermore, assessment of macrophage kinetics after ischemic damage as well as spatiotemporal monitoring of inflammatory activity might gain new insights into the pathophysiology of inflammation and offer a new promising target for both patient monitoring and therapy assessment.

As SSTR-targeted radiotracers for PET/CT imaging are more specific for inflammation and lack physiologic myocardial uptake, they might prove well-suited for specifically visualizing myocardial inflammation. Therefore, we investigated the concept of macrophage detection with SSTR-PET/CT in comparison to cardiac MRI in patients with sub-acute myocardial infarction and acute peri-/myocarditis, respectively. Our hypothesis was that SSTR-PET/CT provides complementary information to MRI for imaging myocardial inflammation.

2. Materials and methods

2.1. Subjects and study design

From December 2013 to June 2014, a total of 12 patients (7 males and 5 females, mean age, 52 ± 10 years: range, 33–70 years) with the suspicion of inflammatory heart disease underwent both SSTR-PET/CT as well as cardiac MRI on a compassionate use base. Six patients (all male) presented after myocardial infarction diagnosed according to current national and international guidelines [20]. The remaining 6 patients (5 female, 1 male) suffered from acute pericardial or myocardial inflammation as defined by Lake Louise criteria [9]. Imaging was performed within 3–10 days after the onset of symptoms (mean, 7 ± 3 days; delay between PET and MRI, 3 ± 3 days).

German federal laws accept the use of the radiotracer ^{68}Ga-DOTA-TOC under conditions of the pharmaceutical law. The local ethics committee granted compassionate use of ^{68}Ga-DOTA-TOC-PET/CT in a limited number of pilot patients. Written informed consent was obtained prior to imaging from all patients.

2.2. Preparation of ^{68}Ga-DOTA-TOC

^{68}Ga-DOTA-TOC was prepared using a modification of the method described previously by Breeman et al. [21] using a SCINTOMICS module (Scintomics, Fürstenfeldbruck, Germany). The synthesis was carried out on a computer-assisted synthesis module (Scintomics, Fürstenfeldbruck, Germany). The labeling procedure was optimized concerning amount of peptide, reaction time and reaction temperature. Radiochemical purity was determined by gradient HPLC (Scintomics, Fürstenfeldbruck, Germany).

2.3. PET imaging

PET scans were acquired using an integrated PET/CT scanner (Siemens Biograph mCT 64, Siemens, Knoxville, USA) consisting of a LSO full-ring PET and a 64-slice spiral CT. 104 ± 30 MBq of ^{68}Ga-DOTA-TOC was injected. After a period of 60 min, transmission data were acquired using low-dose CT of the thorax (80 mAs, 120 kV, 512 × 512 matrix, 5 mm slice thickness, increment of 30 mm/s, rotation time of 0.5 s, and pitch index of 0.8). Consecutively, PET emission data were acquired in three-dimensional mode with a 200 × 200 matrix with 10 min emission time. After decay and scatter correction, PET data were reconstructed iteratively with attenuation correction using a dedicated software (HD PET, Siemens Esoft).

Images were first inspected visually by two experienced nuclear medicine physicians (CL and AKB). For quantification of increased tracer uptake, a visual score using the terms “mild”, “moderate” and “intense” was used. Areas of increased ^{68}Ga-DOTA-TOC accumulation were documented using the 17-segment AHA heart model [22].

For semi-quantitative analysis, the axial PET image slice with maximum cardiac uptake was selected. A standardized 15 mm circular region was placed over the area with the peak activity. This first ROI was used to derive maximum (SUV_{max}) and mean standardized uptake values (SUV_{mean}). SUV_{max} and SUV_{mean} were also derived in normal reference regions defined by two distinct methods: (1) a second ROI (diameter of 15 mm) in a remote region of the left ventricular wall without late-gadolinium-enhancement (LGE) in the corresponding MRI data (if applicable) and (2) another ROI with a diameter of 25 mm in the left ventricular cavity. Signal-to-background ratios were calculated for each method.

For inter-individual comparison, 20 consecutive oncologic patients (12 males; 8 females; mean age, 53 ± 13 years) with no history of coronary artery disease or other known cardiac disease undergoing SSTR-PET/CT (120 ± 27 MBq ^{68}Ga-DOTA-TOC) for staging purposes were enrolled. In this patient cohort, imaging started 45–60 min after tracer injection with 2 min emission time per bed position. As for the infarction/myocarditis cohort, cardiac uptake was defined by placing a ROI with a diameter of 15 mm in the left lateral ventricular wall.

2.4. MRI imaging

MRI was performed on a 1.5 T scanner (Achieva 1.5 T, Philips Healthcare, Best, The Netherlands), using a 32 element phased array coil for radiofrequency reception. Sequences were gated to the heart cycle via a four lead vector cardiogram. The protocol included a morphologic study based on balanced turbo field echo sequences for documentation of standard cine long and short axis views (FOV 380 mm, flip angle 60°, TE 2.6–3.0 ms, TR 130–158 ms). A T2-weighted multi-echo gradient echo sequence was used for imaging myocardial edema in both long and short axes (FOV 370 ms, NSA 2, TE 90 ms, TR 2000–3600 ms, TR (beats) 3). Late enhancement imaging was performed 9 to 12 min after antecubital intravenous administration of 0.15 mmol/kg of a gadolinium based contrast agent (Gadobutrol, Bayer HealthCare, Leverkusen, Germany). An inversion recovery T1 turbo field echo sequence was used, and the inversion time was adjusted to completely null the myocardial signal.

Image analysis was performed using the Extended Workspace software (EWS, Philips Healthcare, Best, The Netherlands) and followed European standards [23]. In analogy to PET, all LGE scans were segmentally analyzed with regard to scar distribution within the myocardium according to the 17-segment model.

2.5. Statistical analysis

Quantitative data are presented as median, range, and mean ± SD. The Wilcoxon signed rank test and the Mann–Whitney test were used for paired and unpaired comparisons of quantitative parameters. Statistical analyses were performed using SPSS Statistics software for Windows (version 22.0, SPSS Inc., Chicago, USA). All statistical tests were performed two-sided and a p-value < 0.05 was considered statistically significant.

Table 1
Clinical and laboratory features obtained at admission (7 ± 3 days prior to imaging).

No.	Sex	Age	Clinical diagnosis (occluded vessel)	Troponin [pg/ml]	CK/CK-MB [U/l]	LDH [U/l]
1	F	50	Myocarditis	972	783/105	391
2	F	45	Pericarditis	N/A	21	344
3	F	33	Myocarditis	N/A	728/70	277
4	F	54	Sarcoidosis	38.5	65	189
5	M	52	Sarcoidosis	506	281/36	445
6	F	70	Myocarditis	136	44	209
7	M	52	Infarction (LAD, LCX)	317	512/69	194
8	M	56	Infarction (LCX)	N/A	303	695
9	M	65	Infarction (LAD, LCX)	535	680/53	695
10	M	44	Infarction (LAD, LCX)	N/A	293/n.n	683
11	M	48	Infarction (RCA)	2745	952/153	282
12	M	58	Infarction (LAD)	7800	2365/471	966

LAD: left anterior descending artery; LCX: left circumflex coronary artery; N/A: not available; RCA: right coronary artery.

3. Results

3.1. Clinical findings

Basic clinical and laboratory findings of the cohort are summarized in Table 1. All patients presented with acute chest pain and elevated cardiac enzymes (troponin T, creatinine kinase). In 7 patients, electrocardiograms (ECG) demonstrated ST segment elevations suspicious for acute myocardial infarction. Left bundle branch block was detected in one subject. The remaining 4 patients had non-specific ECG alterations. Subsequently, in all patients, interventional coronary angiography was performed and revealed coronary vessel occlusion in 6 patients. Two patients had involvement of 2 vessels, and the remainder suffered from occlusion of a single coronary artery. The left anterior descendant artery (LAD) was affected in 3 cases, the left coronary circumflex (LCX) in 2 and the right coronary artery (RCA) in 3 subjects, respectively. In the remaining 6 patients, coronary heart disease was excluded by coronary angiography. Next, cardiac MRI was performed and suggested acute myocardial inflammation. Global systolic LV function was normal in all but one patient; regional wall motion abnormalities were associated with the distribution pattern of scarring. In 2 patients (1 male, 52 years; 1 female, 54 years), bronchial lavage and biopsy furnished evidence of acute sarcoidosis.

Twenty patients who underwent SSTR-PET/CT for staging of neuroendocrine cancer served as reference. In all of these patients, no clinical signs of cardiac disease and no history of cardiac events were recorded. SSTR-PET/CT displayed no areas of focal or diffuse cardiac tracer uptake (Fig. 1).

3.2. Imaging results

Both SSTR-PET/CT and MRI returned positive findings in all patients (sensitivity for both modalities, 100%; see Table 2). In a total of 204 segments analyzed, there were 55 segments positive in ^{68}Ga-DOTA-TOC-PET/CT and 44 segments positive in MRI, respectively. In patients with clinical evidence of myocarditis, PET/CT returned 26 positive segments and MRI 13 segments, respectively. In patients with myocardial infarction, there were 29 ^{68}Ga-DOTA-TOC positive segments and 31 abnormal segments in MRI. In a single patient with pericarditis, circular tracer retention was obvious at ^{68}Ga-DOTA-TOC-PET/CT, sparing the myocardium. Correspondingly, prominent pericardial enhancement was described at MRI. Overall, retention of the radiotracer ^{68}Ga-DOTA-TOC was rated mild or moderate and no segment was rated intense (mild retention in 21/55 (38%) segments; moderate retention, 32/55; 62%). Typical PET-findings illustrating enhanced tracer uptake in both myocarditis/sarcoidosis as well as in acute myocardial infarction are given in Figs. 2 and 3, respectively.

On a head-to-head comparison, SSTR-PET and MRI were concordantly positive in 36 segments (36/47 segments positive at MRI; 76.6%). 19 segments were SSTR-PET positive and MRI-negative (9.3%; 19/204), and 11 SSTR-PET negative and MRI-positive (5.4%; 11/204). Both modalities returned negative results in 138 segments, thus leading to an overall concordance of 85.3%. Agreement of the modalities was higher in patients with myocardial infarctions (see Table 3). The individual results of the 17-segment analysis for both sub-groups can be inferred from Supplementary Figs. 1 and 2.

3.3. Semi-quantitative analysis

SUV_{mean} and SUV_{max} were significantly higher in the infarcted/inflamed myocardium as compared to remote myocardium or the left ventricular (LV) cavity. SUV_{mean} in infarcted/inflamed areas ranged from 2.2 to 5.2 (mean, 3.5 ± 0.9) and SUV_{max} from 2.4 to 6.1 (mean, 4.0 ± 1.1), respectively. The SUV_{mean} ratios of lesion-to-remote myocardium were 1.9 ± 0.4 and for lesion-to-LV cavity 1.9 ± 0.3. The corresponding SUV_{max} ratios were 1.8 ± 0.3 and 1.7 ± 0.3, respectively. Patients with cardiac disease showed almost doubled tracer uptake even in remote myocardial areas as compared to oncology patients undergoing SSTR-PET for staging purposes (SUV_{mean}, 1.8 ± 0.4 vs. 0.9 ± 0.2; SUV_{max}, 2.2 ± 0.4 vs. 1.4 ± 0.4, $p < 0.01$, respectively).

4. Discussion

Our results further support the concept of somatostatin receptor directed PET imaging as a readout of macrophage infiltration within areas of inflamed and/or damaged myocardium. Patients with active

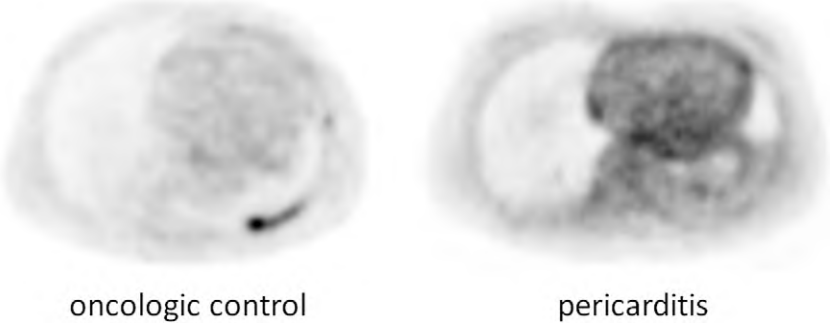

Fig. 1. Increased retention of ^{68}Ga-DOTA-TOC as compared to normal myocardium. The figure shows an example of an 50-year-old patient with a history of pleura carcinosis due to atypical carcinoid of the lung (left) in comparison to an 45 year-old female with the diagnosis of acute pericarditis and circular tracer retention (right). Moderately intense tracer retention can be seen in the pericardium (right) as compared to the cavity of the left ventricle. In the control scan (left), no tracer retention in the peri-/ myocardium can be detected.

Table 2
MRI and visual PET findings in myocarditis and myocardial infarction.

No	Ejection fraction	Wall motion abnormalities	T2-weighted images	Late enhancement	SSTR-PET
Myocarditis					
1	69%	None	Lat and AL apical, subepicardial	Lat, AL/PL apical, subepicardial, intramural	Lat and AL apical
2	55%	None	Pericardial	Pericardial, Lat, Inf	Pericardial diffuse
3	64%	Inf midbasal, Lat apical–midbasal	Inf midbasal, Lat	Inf midbasal, Lat inhomogenous	Myocardial diffuse
4	39%	Sep, Ant basal–midbasal	Sep, Ant basal–midbasal	Sep, Ant basal–midbasal, inhomogenous	Sep, Ant, AS
5	67%	None	Lat midbasal–apical, epicardial	Lat midbasal, apical	Lat midbasal
6	66%	Inf midbasal	Lat midbasal to apical	Lat midbasal	Lat midbasal
Myocardial infarction					
1	52%	Inf basal	Inf basal–midbasal	Inf basal–midbasal, transmural	Inf basal
2	55%	Inf, PL midbasal	Not acquired	Inf apical–basal, transmural MVO	Inf, IL
3	42%	Inf, IL	Inf, IS, IL	Inf, IS, IL, transmural, MVO	Inf, IL
4	31%	Ant apical–midbasal, Inf and Lat apical	Ant, Sep, Inf and Lat apical–midbasal	Ant, Sep, Inf and Lat apical–midbasal/basal, transmural, MVO	Ant and Lat apical–midbasal, Inf apical
5	58%	Inf apical	Inf apical	Inf apical–basal, transmural	Inf midbasal–basal
6	56%	Ant and Sep	Ant	Ant and AS with MVO, transmural	Ant and AS apical–midbasal

AL, anterolateral; Ant, anterior; AS, anteroseptal; Inf, inferior; IS, inferoseptal; Lat, lateral; MVO, microvascular obstruction; PL, posterolateral; Sep, septal.

myocarditis or sub-acute myocardial infarction invariably showed cardiac accumulation of the radiotracer ^{68}Ga-DOTA-TOC. In contrast, patients undergoing SSTR-PET/CT for cancer imaging – serving as control – revealed no significant cardiac tracer uptake, indicating specificity of tracer retention in inflammatory lesions of the heart. Distribution of the radiotracer matched with MRI late-gadolinium-enhancement and T2-weighted edema, demonstrating focal accumulation within areas of acute myocardial damage in 36 of 47 involved segments (76.6%). Tracer uptake in damaged myocardium was twice as high as compared to the background of left the ventricular cavity or remote unaffected myocardium. Interestingly, tracer uptake in remote, non-ischemic myocardial areas was higher in myocardial infarction patients than in the control group. This finding supports the hypothesis of general inflammation of the left ventricular myocardium following acute ischemic damage.

Abundant extravascular macrophages have been revealed in the healthy heart [24]. Under steady state conditions, they are not particularly "inflammatory", however, upon inflammatory stimuli, capillaries in the remote zone increase chemokine expression and recruit monocytes [25,26]. Compared with ischemic myocardium, remote

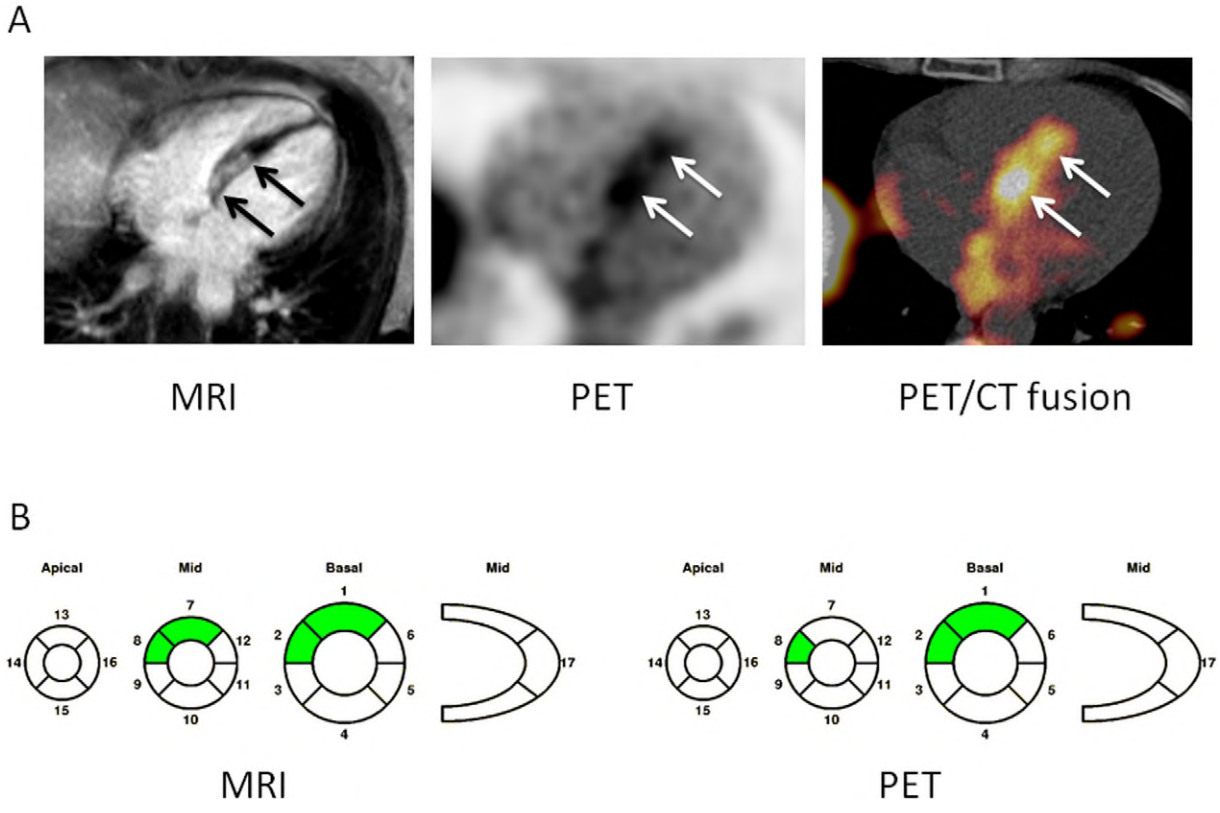

Fig. 2. Increased ^{68}Ga-DOTA-TOC uptake in acute myocarditis/cardiac sarcoidosis (54 year-old female with biopsy-confirmed sarcoidosis; patient #4). (A) Axial slices of both contrast-enhanced T2-weighted MRI, SSTR-PET as well as fused PET/CT and (B) corresponding analysis using a 17-segment heart model. Images reveal increased ^{68}Ga-DOTA-TOC uptake in the septum that consistently matches areas of septal myocardial damage in MRI (arrows). There is remarkable overlap in the affected segments (B).

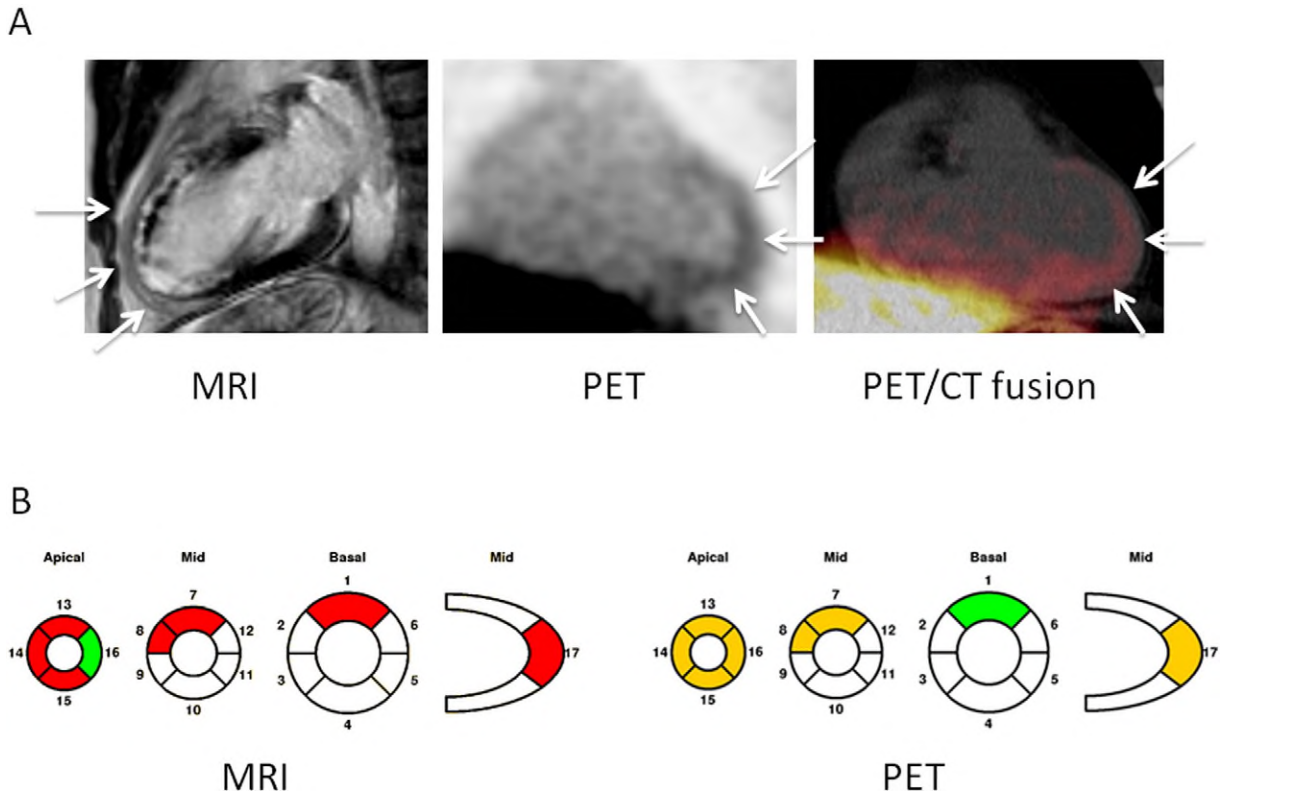

Fig. 3. Increased 68Ga-DOTA-TOC uptake after acute myocardial infarction (58 year-old male patient with acute infarction of the left anterior descendant coronary artery; patient #12). (A) Long-axis slice of the contrast-enhanced T1-weighted MRI scan, coronal slices of both SSTR-PET and fused PET/CT and (B) corresponding analysis using a 17-segment heart model. Images demonstrate increased 68Ga-DOTA-TOC uptake in the apex and septal/anterior wall that consistently matches MRI (arrows and B); green segments signify 1–25% infarction thickness (MRI) and weak tracer accumulation (PET), respectively; yellow segments denote moderate tracer accumulation (SSTR-PET), red segments illustrate 75–100% infarction thickness (MRI).

myocardium accumulates monocytes and macrophages more slowly. Remote zone macrophage numbers peak only around day 10 after ischemic damage [25]. In our cohort, the interval between the ischemic event and PET averaged 7 ± 3 days. Therefore, the higher tracer uptake in remote myocardium might reflect an increased number of activated macrophages also infiltrating these non-damaged areas [25].

However, as the oncologic imaging protocol differed from the dedicated cardiac protocol in terms of delay after tracer injection and time per bed position during the scan, at least parts of the observed differences might be artificial. Further analysis is warranted in future studies.

Up to now, only few studies have addressed the value of SSTR-PET/CT for the imaging of cardiovascular inflammation. Most reports have focused on the detection of atherosclerotic plaques within the vessel walls and demonstrated the feasibility of SSTR-PET/CT for characterizing biological activity of atherosclerotic plaque via SSTR-2 expression and hinted at SSTR-directed therapies in high-risk atherosclerosis [18,19,27].

In its translation to the setting of myocardial inflammation, this approach might allow for direct assessment of the spatiotemporal distribution of macrophages in the course of cardiac inflammatory processes which is not achieved by any other imaging technique so far. While the current gold standard MRI depicts structural changes like cardiac damage and scarring with the highest spatial resolution, ^{68}Ga-DOTA-TOC uptake may reflect the directly underlying immunological cell activity. In future, given the complementary nature of PET and MRI signals, the combination of the two may be the optimal diagnostic approach, preferably by integrated MRI/PET.

Our work has several limitations. Most importantly, histopathologic proof of macrophage infiltration and SSTR expression as adequate reference test was not available in the entire study population. Study numbers of this pilot study are rather small and the etiology of cardiac inflammation varies as patients with viral myocarditis and cardiac sarcoidosis were enrolled. Furthermore, macrophage kinetics was not directly followed. However, previous studies have demonstrated that macrophages infiltrate the ischemic myocardium within the first two weeks after infarction [25]. Next, due to the high physiologic ^{68}Ga-DOTA-TOC uptake of normal liver parenchyma, delineation of inferior wall abnormalities is rather challenging. New tracers with less non-specific liver uptake would be clearly beneficial.

Table 3
Concordance of cardiac MRI and somatostatin-receptor- (SSTR-) based PET/CT for involved myocardial segments in the overall cohort as well as for the myocarditis and infarction sub-groups as derived from the 17-segment model of the heart. Inter-modality agreement reaches 85.3% (174/204 segments) for the overall collective, 81.4% (83/102) for myocarditis, and 89.2% (91/102) for myocardial infarction.

		Cardiac MRI		∑
		Positive	Negative	
Myocarditis (n = 6)				
SSTR-PET	Positive	10	16	26
	Negative	3	73	76
∑		13	89	102
Myocardial infarction (n = 6)				
SSTR-PET	Positive	26	3	29
	Negative	8	65	73
∑		34	68	102
Total collective (n = 12)				
SSTR-PET	Positive	36	19	55
	Negative	11	138	149
∑		47	157	204

Data on short-term reproducibility of our findings are missing and should be the subject of subsequent work. Finally, the PET imaging protocols for the oncologic control group and the cardiac inflammation group slightly differed in the timing of scanning after tracer injection and might limit direct comparability with the myocarditis/infarction group. Nevertheless, more targeted imaging of monocyte/macrophage activity within sub-acutely infarcted or inflamed myocardium might be feasible by using SSTR-analogs and should be further assessed in larger clinical studies. In the future, potential further scenarios for inflammation imaging with SSTR-directed radiocompounds can be speculated on. For example, SSTR-based imaging might help in the detection of endocarditis (though small lesions sizes and motion artifacts might limit its utility). Another possible application might include the visualization of pathophysiology of toxic cardiomyopathies including acute alcohol exposure or acute adverse responses to chemotherapy.

5. Conclusion

SSTR-targeted imaging using PET/CT may have a complementary role to cardiac MRI for imaging myocardial inflammation in the course of acute myocarditis and/or sub-acute infarction. Our pilot data warrant further analysis in a larger prospective series.

Supplementary data to this article can be found online at http://dx.doi.org/10.1016/j.ijcard.2015.05.073.

Conflicts of interest

All authors declare no conflicts of interest.

Acknowledgments

This study was supported by the Deutsche Forschungsgemeinschaft (SFB688, Z02; TP B05) and the Bundesministerium für Bildung und Forschung (BMBF01, EO1004).

References

[1] S. Frantz, M. Nahrendorf, Cardiac macrophages and their role in ischaemic heart disease, Cardiovasc. Res. 102 (2014) 240–248.
[2] A.M. van der Laan, E.N. Ter Horst, R. Delewi, M.P. Begieneman, P.A. Krijnen, A. Hirsch, M. Lavaei, M. Nahrendorf, A.J. Horrevoets, H.W. Niessen, J.J. Piek, Monocyte subset accumulation in the human heart following acute myocardial infarction and the role of the spleen as monocyte reservoir, Eur. Heart J. 35 (2014) 376–385.
[3] M. Nahrendorf, F.K. Swirski, E. Aikawa, L. Stangenberg, T. Wurdinger, J.L. Figueiredo, P. Libby, R. Weissleder, M.J. Pittet, The healing myocardium sequentially mobilizes two monocyte subsets with divergent and complementary functions, J. Exp. Med. 204 (2007) 3037–3047.
[4] M. Nahrendorf, M.J. Pittet, F.K. Swirski, Monocytes: protagonists of infarct inflammation and repair after myocardial infarction, Circulation 121 (2010) 2437–2445.
[5] Y.X. Ye, T.C. Basse-Lüsebrink, P.A. Arias-Loza, V. Kocoski, T. Kampf, Q. Gan, E. Bauer, S. Sparka, X. Helluy, K. Hu, K.H. Hiller, V. Boivin-Jahns, P.M. Jakob, R. Jahns, W.R. Bauer, Monitoring of monocyte recruitment in reperfused myocardial infarction with intramyocardial hemorrhage and microvascular obstruction by combined fluorine 19 and proton cardiac magnetic resonance imaging, Circulation 128 (2013) 1878–1888.
[6] M. Guglin, L. Nallamshetty, Myocarditis: diagnosis and treatment, Curr. Treat. Options Cardiovasc. Med. 14 (2012) 637–651.
[7] L.T. Cooper, K.L. Baughman, A.M. Feldman, A. Frustaci, M. Jessup, U. Kuhl, G.N. Levine, J. Narula, R.C. Starling, J. Towbin, R. Virmani, The role of endomyocardial biopsy in the management of cardiovascular disease: a scientific statement from the American Heart Association, the American College of Cardiology, and the European Society of Cardiology Endorsed by the Heart Failure Society of America and the Heart Failure Association of the European Society of Cardiology, Eur. Heart J. 28 (2007) 3076–3093.
[8] M. Kasner, D. Sinning, F. Escher, D. Lassner, U. Kühl, H.P. Schultheiss, C. Tschöpe, The utility of speckle tracking imaging in the diagnostic of acute myocarditis, as proven by endomyocardial biopsy, Int. J. Cardiol. 168 (2013) 3023–3024.
[9] M.G. Friedrich, U. Sechtem, J. Schulz-Menger, G. Holmvang, P. Alakija, L.T. Cooper, J.A. White, H. Abdel-Aty, M. Gutberlet, S. Prasad, A. Aletras, J.P. Laissy, I. Paterson, N.G. Filipchuk, A. Kumar, M. Pauschinger, P. Liu, International Consensus Group on Cardiovascular Magnetic Resonance in Myocarditis, Cardiovascular magnetic resonance in myocarditis: a JACC White Paper, J. Am. Coll. Cardiol. 53 (2009) 1475–1487.
[10] S.C. Bekkers, S.K. Yazdani, R. Virmani, J. Waltenberger, Microvascular obstruction: underlying pathophysiology and clinical diagnosis, J. Am. Coll. Cardiol. 55 (2010) 1649–1660.
[11] J. Meller, C.-O. Sahlmann, A.K. Scheel, 18F-FDG PET and PET/CT in fever of unknown origin, J. Nucl. Med. 48 (2007) 35–45.
[12] B.C. Millar, B.D. Prendergast, A. Alavi, J.E. Moore, ^{18}FDG-positron emission tomography (PET) has a role to play in the diagnosis and therapy of infective endocarditis and cardiac device infection, Int. J. Cardiol. 167 (2013) 1724–1736.
[13] K. Ozawa, N. Funabashi, M. Daimon, H. Takaoka, H. Takano, M. Uehara, Y. Kobayashi, Determination of optimum periods between onset of suspected acute myocarditis and ^{18}F-fluorodeoxyglucose positron emission tomography in the diagnosis of inflammatory left ventricular myocardium, Int. J. Cardiol. 169 (2013) 196–200.
[14] C. Anagnostopoulos, A. Georgakopoulos, N. Pianou, S.G. Nekolla, Assessment of myocardial perfusion and viability by positron emission tomography, Int. J. Cardiol. 167 (2013) 1737–1749.
[15] P. Iozzo, P. Chareonthaitawee, M. Di Terlizzi, D.J. Betteridge, E. Ferrannini, P.G. Camici, Regional myocardial blood flow and glucose utilization during fasting and physiological hyperinsulinemia in humans, Am. J. Physiol. Endocrinol. Metab. 282 (2002) E1163–E1171.
[16] V.A. Dalm, P.M. van Hagen, P.M. van Koetsveld, S. Achilefu, A.B. Houtsmuller, D.H. Pols, A.J. van der Lely, S.W. Lamberts, L.J. Hofland, Expression of somatostatin, cortistatin, and somatostatin receptors in human monocytes, macrophages, and dendritic cells, Am. J. Physiol. Endocrinol. Metab. 285 (2003) E344–E353.
[17] C. Armani, E. Catalani, A. Balbarini, P. Bagnoli, D. Cervia, Expression, pharmacology, and functional role of somatostatin receptor subtypes 1 and 2 in human macrophages, J. Leukoc. Biol. 81 (2007) 845–855.
[18] X. Li, S. Samnick, C. Lapa, I. Israel, A.K. Buck, M.C. Kreissl, W. Bauer, ^{68}Ga-DOTATATE PET/CT for the detection of inflammation of large arteries: correlation with ^{18}F-FDG, calcium burden and risk factors, EJNMMI Res. 2 (2012) 52.
[19] X. Li, W. Bauer, M.C. Kreissl, J. Weirather, E. Bauer, I. Israel, D. Richter, G. Riehl, A. Buck, S. Samnick, Specific somatostatin receptor II expression in arterial plaque: (68)Ga-DOTATATE autoradiographic, immunohistochemical and flow cytometric studies in apoE-deficient mice, Atherosclerosis 230 (2013) 33–39.
[20] K. Thygesen, J.S. Alpert, A.S. Jaffe, M.L. Simoons, B.R. Chaitman, H.D. White, Joint ESC/ACCF/AHA/WHF Task Force for Universal Definition of Myocardial Infarction, Authors/Task Force Members Chairpersons, K. Thygesen, J.S. Alpert, H.D. White, Biomarker Subcommittee, A.S. Jaffe, H.A. Katus, F.S. Apple, B. Lindahl, D.A. Morrow, ECG Subcommittee, B.R. Chaitman, P.M. Clemmensen, P. Johanson, H. Hod, Imaging Subcommittee, R. Underwood, J.J. Bax, J.J. Bonow, F. Pinto, R.J. Gibbons, Classification Subcommittee, K.A. Fox, D. Atar, L.K. Newby, M. Galvani, C.W. Hamm, Intervention Subcommittee, B.F. Uretsky, P.G. Steg, W. Wijns, J.P. Bassand, P. Menasche, J. Ravkilde, Trials & Registries Subcommittee, E.M. Ohman, E.M. Antman, L.C. Wallentin, P.W. Armstrong, M.L. Simoons, Trials & Registries Subcommittee, J.L. Januzzi, M.S. Nieminen, M. Gheorghiade, G. Filippatos, Trials & Registries Subcommittee, R.V. Luepker, S.P. Fortmann, W.D. Rosamond, D. Levy, D. Wood, Trials & Registries Subcommittee, S.C. Smith, D. Hu, J.L. Lopez-Sendon, R.M. Robertson, D. Weaver, M. Tendera, A.A. Bove, A.N. Parkhomenko, E.J. Vasilieva, S. Mendis, ESC Committee for Practice Guidelines (CPG), J.J. Bax, H. Baumgartner, C. Ceconi, V. Dean, C. Deaton, R. Fagard, C. Funck-Brentano, D. Hasdai, A. Hoes, P. Kirchhof, J. Knuuti, P. Kolh, T. McDonagh, C. Moulin, B.A. Popescu, Z. Reiner, U. Sechtem, P.A. Sirnes, M. Tendera, A. Torbicki, A. Vahanian, S. Windecker, Document Reviewers, J. Morais, C. Aguiar, W. Almahmeed, D.O. Arnar, F. Barili, K.D. Bloch, A.F. Bolger, H.E. Botker, B. Bozkurt, R. Bugiardini, C. Cannon, J. de Lemos, F.R. Eberli, E. Escobar, M. Hlatky, S. James, K.B. Kern, D.J. Moliterno, C. Mueller, A.N. Neskovic, B.M. Pieske, S.P. Schulman, R.F. Storey, K.A. Taubert, P. Vranckx, D.R. Wagner, Third universal definition of myocardial infarction, J. Am. Coll. Cardiol. 6 (2012) 1581–1598.
[21] W.A. Breeman, E. de Blois, H. Sze Chan, M. Konijnenberg, D.J. Kwekkeboom, E.P. Krenning, (68)Ga-labeled DOTA-peptides and (68)Ga-labeled radiopharmaceuticals for positron emission tomography: current status of research, clinical applications, and future perspectives, Semin. Nucl. Med. 41 (2011) 314–321.
[22] American Society of Nuclear Cardiology, Imaging guidelines for nuclear cardiology procedures, Part 2, J. Nucl. Cardiol. 6 (1999) G47–G84.
[23] J. Schulz-Menger, D.A. Bluemke, J. Bremerich, S.D. Flamm, M.A. Fogel, M.G. Friedrich, R.J. Kim, F. von Knobelsdorff-Brenkenhoff, C.M. Kramer, D.J. Pennell, S. Plein, E. Nagel, Standardized image interpretation and post processing in cardiovascular magnetic resonance: Society for Cardiovascular Magnetic Resonance (SCMR) board of trustees task force on standardized post processing, J. Cardiovasc. Magn. Reson. 15 (2013) 35.
[24] A.R. Pinto, R. Paolicelli, E. Salimova, J. Gospocic, E. Slonimsky, D. Bilbao-Cortes, J.W. Godwin, N.A. Rosenthal, An abundant tissue macrophage population in the adult murine heart with a distinct alternatively-activated macrophage profile, PLoS One 7 (2012) e36814.
[25] W.W. Lee, B. Marinelli, A.M. van der Laan, B.F. Sena, R. Gorbatov, F. Leuschner, P. Dutta, Y. Iwamoto, T. Ueno, M.P. Begieneman, H.W. Niessen, J.J. Piek, C. Vinegoni, M.J. Pittet, F.K. Swirski, A. Tawakol, M. Di Carli, R. Weissleder, M. Nahrendorf, PET/MRI of inflammation in myocardial infarction, J. Am. Coll. Cardiol. 59 (2012) 153–163.
[26] O. Borst, M. Schaub, B. Walker, M. Sauter, P. Muenzer, M. Gramlich, K. Mueller, T. Geisler, F. Lang, K. Klingel, R. Kandolf, B. Bigalke, M. Gawaz, C.S. Zuern, CXCL16 is a novel diagnostic marker and predictor of mortality in inflammatory cardiomyopathy and heart failure, Int. J. Cardiol. 176 (2014) 896–903.
[27] I. Schatka, T. Wollenweber, C. Haense, F. Brunz, K.F. Gratz, F.M. Bengel, Peptide receptor-targeted radionuclide therapy alters inflammation in atherosclerotic plaques, J. Am. Coll. Cardiol. 62 (2013) 2344–2345.